Integrated Control of a Motor/Generator Set Composed of Doubly-Fed Induction Machines

Marc Bodson, *Fellow, IEEE,* and Md Abid Hossain
Department of Electrical & Computer Engineering
University of Utah, Salt Lake City, USA

***Abstract*— The paper considers the control problem for a motor/generator set where a prime mover drives a generator and the electrical power produced drives a motor. Both the generator and the motor are assumed to be doubly-fed induction machines with direct AC connection between their stators. The rotors are controlled by three-phase converters, so that operation is possible with motor and generator speeds that are different from each other, and not synchronized with the electrical frequency of the stator voltages. The strong couplings between the two machines motivate the design of an integrated controller. The paper proposes a general framework for a such design, based on a joint model of the two machines. A specific method is also developed for the control of the stator voltages and the motor velocity. In its simplest form, the proposed algorithm does not rely on current sensors. A current command option is also developed that ensures closer tracking and limiting of the rotor currents. The algorithm is relatively simple and all its parameters can be computed based on estimates of the machine parameters. Practical implementation and testing can be performed rapidly. Experiments performed on a small-scale laboratory testbed show very good tracking performance of a speed reference profile.**

Corresponding author information: **Professor M. Bodson, Department of Electrical and Computer Engineering, University of Utah, 50 S Central Campus Dr, Rm 2110, Salt Lake City, UT 84112, U.S.A. E-mail: bodson@eng.utah.edu. Phone: (801) 581 8590.**

I. Introduction

The paper considers the energy conversion system shown on Fig. 1, which involves a doubly-fed induction generator (DFIG) and a doubly-fed induction motor (DFIM). An application to hybrid electric propulsion for aircraft is envisioned, but other applications are possible as well. The generator absorbs mechanical power from a prime mover and generates electrical power. The–motor converts the electrical power back into mechanical power and applies it to a load. The speed of the prime mover and of the load can be different, which means that the motor/generator set can be viewed as a special type of variable speed transmission. With a gas turbine as prime mover and a propulsor as load, motor/generator systems of this type are being considered as new propulsion solutions for future aircraft. Electric propulsion would enable novel airplane configurations, possibly increasing efficiency and reducing noise as well as pollution.

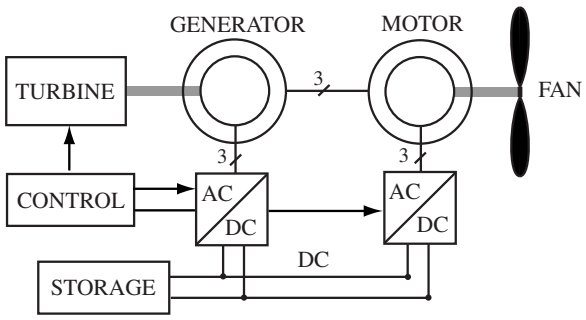

Fig. 1. Motor/generator set with doubly-fed induction machines

In an implementation comparable to existing hybrid electric cars, AC power would be produced by a generator, converted to DC, and then back to AC with variable voltage and frequency to drive an electric motor. Two power electronic converters would be needed at the full rated power. The alternative concept proposed in [1] and represented in Fig. 1 is such that power is transferred without conversion from the stator of one machine to the other. Power electronic converters are needed for generator and motor control (through the rotors), but involve only a fraction of the total power transferred for a range of operating condtions. This property of the machines is the reason behind the prevalence of doubly-fed induction generators in wind power [2].

The control of a motor/generator set presents challenges that have not received much attention before. While decoupled control of the motor and generator is possible, large demands from the load may produce significant drops in the AC bus voltage and deteriorate the load speed regulation. The problem can be alleviated if energy storage is included between the motor and the generator. In this context, [3] proposes a methodology to manage the transfer of energy between motor, generator, and storage. Under consideration is an architecture with DC link and full power converters. Conversely, [4] considers the coordination of two doubly-fed induction

generators in a stator connection similar to Fig. 1, but without a variable motor load.

The system as shown on Fig. 1 was considered in [5], with a power supply replacing the generator and with multiple motors placed in parallel. Experiments performed afterwards with a generator controlled independently from the motors showed good results but also visible drops of stator voltage when the motors accelerated rapidly [6]. The method proposed in this paper coordinates the control of the generator and of the motor so that the rotor side converters control *together* the torque applied to the load *and* the AC bus voltage. One device does not react to the actions of the other. Instead, their actions are coordinated and the controllers for the two machines are integrated into a single motor/generator controller.

In order to approach the control problem, the paper adopts a complex variable representation of the doubly-fed induction machines. The use of such models for steady-state analysis is common, but is less typical for transient analysis, although not new [7]. Yet, various applications have emerged over the years, especially in energy systems [8], but also in signal processing and some mechanical systems [9]. Increasingly, the complex representation is used not only to simplify the equations of the system, but also to design and implement control systems [10], [11], [12]. The controllers developed in this paper were coded using complex arithmetic, with real/complex and complex/real interfaces to the signals from the sensors and to the actuators. Increasingly, algorithms are also analyzed in the complex domain using frequency-domain and Nyquist tools [13], and complex root-locus methods [14]. In some cases, results were obtained that were not known or could not be derived in the real domain [15], [16].

The paper first develops an integrated model of the combined motor/generator set that accounts for the stator voltages and currents of the two machines being equal (except for a sign change for the currents). The original electrical model of the motor/generator set in DQ variables has a total of eight differential equations. With the integrated representation using complex variables, a model with only three differential equations is obtained. Through this considerable reduction in size of the model, an integrated control algorithm is derived that is remarkably simple and effective. Two options are considered: the first is referred to as the voltage command mode and does not measure the rotor currents, while the second called the current command mode uses measurements of the rotor currents to actively control these currents and limit their amplitude for the protection of the converters. The control methods are tested successfully on an experimental testbed and the data demonstrates close tracking of a speed profile by the motor. The results are achieved with the speed of the generator following a different profile than the motor, and operation alternating between sub-synchronous and super-synchronous modes at different times on the motor and the generator sides.

II. Model of the Motor/Generator Set

A. Three-phase to complex transformation

A doubly-fed induction machine with three stator windings and three rotor windings is considered. The voltages applied to the stator windings are denoted v_{SA}, v_{SB}, v_{SC}, while the currents flowing in the windings are denoted i_{SA}, i_{SB}, i_{SC} (with the convention that power is absorbed by the winding if the product of voltage times current is positive). Similarly, the voltages applied to the rotor windings are denoted v_{RX}, v_{RY}, v_{RZ}, with the currents flowing into the windings denoted i_{RX}, i_{RY}, i_{RZ}.

The mechanical position is determined by the angle θ (in rad) between winding X of the rotor and winding A of the stator. The mechanical speed is denoted $\omega = d\theta/dt$ (in rad/s).

A *three-phase to complex transformation* (or *3-c transformation*) is applied to the three-phase variables and is defined by

$$v_S = \sqrt{\frac{2}{3}}\ \left(v_{SA} + v_{SB}\ e^{j2\pi/3} + v_{SC}\ e^{-j2\pi/3}\right) e^{-j\theta_S} \tag{1}$$

where θ_S is an electrical angle (in rad) to be defined and v_S is a complex (scalar) signal. The stator currents are transformed using the same 3-c transformation to produce the complex variable i_S. Typically, the complex variable is separated into its real and imaginary components, which are then labelled D and Q, i.e., $v_S = v_{SD} + jv_{SQ}$. If the angle θ_S is chosen such that $v_{SQ} = 0$, the frame of reference is said to be oriented on the stator voltage. In this paper, the angle θ_S is chosen such that the orientation is on the *commanded* stator voltage, rather than the actual stator voltage.

For the rotor variables, the 3-c transformation uses a different angle θ_R (in rad), so that

$$v_R = \sqrt{\frac{2}{3}}\ \left(v_{RX} + v_{RY}\ e^{j2\pi/3} + v_{RZ}\ e^{-j2\pi/3}\right) e^{-j\theta_R} \tag{2}$$

where

$$\theta_R = \theta_S - N_P\theta \tag{3}$$

and N_P is the number of pole pairs of the machine.

The following properties of the $3-c$ transformation will be used. Consider the operation in sinusoidal steady-state such that the angular frequency ω_S (in rad/s)

$$\omega_S = \frac{d\theta_S}{dt} \tag{4}$$

is constant. Then, ω_S is also the angular frequency of the stator voltages and currents, and the complex variables v_S and i_S become

$$v_S = \sqrt{\frac{3}{2}} V_{pk}, \quad i_S = \sqrt{\frac{3}{2}} I_{pk} e^{-j\varphi} \tag{5}$$

In other words, v_S and i_S become equal to scaled phasors for v_{SA} and i_{SA} (as well as phasors for v_{SB}, v_{SC}, i_{SB}, and i_{SC}, with phase shifts of $\pm 2\pi/3$). One also has that p_S and q_S, the total active and reactive powers absorbed by the machine, are given by

$$p_S + jq_S = v_S i_S^* = \frac{3}{2} V_{pk} I_{pk} e^{j\varphi} \tag{6}$$

where i_S^* denotes the complex conjugate of i_S. Even though these identities are valid in steady-state, the variables of the complex model $\sqrt{2/3}\,|v_S|$ and $\sqrt{2/3}\,|i_S|$ provide instantaneous estimates of the peak voltage and the peak current, while $\mathrm{Re}(v_S i_S^*)$, and $\mathrm{Im}(v_S i_S^*)$ provide instantaneous estimates of the active power and the reactive power absorbed by the stator of the machine.

B. Complex model of a motor/generator set

1) Model of the doubly-fed induction motor: In the complex coordinates, the model of a doubly-fed induction machine is

$$\begin{aligned} L_S \frac{di_S}{dt} + M \frac{di_R}{dt} &= v_S - Z_S i_S - Z_{MS} i_R \\ M \frac{di_S}{dt} + L_R \frac{di_R}{dt} &= v_R - Z_R i_R - Z_{MR} i_S \end{aligned} \tag{7}$$

where

$$\begin{aligned} Z_S &= R_S + j\omega_S L_S, \;\; Z_{MS} = j\omega_S M \\ Z_R &= R_R + j\omega_R L_R, \;\; Z_{MR} = j\omega_R M \end{aligned} \tag{8}$$

and ω_R is the angular frequency (in rad/s) of rotation of the reference frame for the rotor

$$\omega_R = \omega_S - N_P\, \omega \tag{9}$$

which becomes the slip frequency in steady-state. R_S and R_R are the stator and rotor winding resistances, L_S and L_R are the stator and rotor winding inductances, and M is the mutual inductance between stator and rotor windings when aligned. The torque of the machine is given by

$$\tau_M = n_P M\, \mathrm{Im}\,(i_S i_R^*) \tag{10}$$

and is defined positive if acting in the positive angular direction (motoring). The voltages and currents are complex functions of time, but the mechanical rotor speed ω, the electrical frequencies ω_S and ω_R, and the torque τ_M are real variables. In [17], this model was used to develop a control algorithm for a doubly-fed induction motor. This paper uses similar techniques, but solves the more complicated problem involving a motor/generator set.

2) Model of the doubly-fed induction generator: For the generator, the variables R_S, L_S, M, R_R, L_R, N_P, ω, and ω_R are replaced by R_{SG}, L_{SG}, M_G, R_{RG}, L_{RG}, N_{PG}, ω_G, and ω_{RG}. The variables v_{SG}, i_{SG} are not used, relying instead on the motor/generator connection, which is such that $v_{SG} = v_S$, $i_{SG} = -i_S$. The variables θ_S and ω_S are also used for the reference frame of the generator. The generator model is then

$$\begin{aligned} -L_{SG} \frac{di_S}{dt} + M_G \frac{di_{RG}}{dt} &= v_S + Z_{SG} i_S - Z_{MSG} i_{RG} \\ -M_G \frac{di_S}{dt} + L_{RG} \frac{di_{RG}}{dt} &= v_{RG} - Z_{RG} i_{RG} + Z_{MRG} i_S \end{aligned} \tag{11}$$

where

$$\begin{aligned} Z_{SG} &= R_{SG} + j\omega_S L_{SG}, \;\; Z_{MSG} = j\omega_S M_G \\ Z_{RG} &= R_{RG} + j\omega_{RG} L_{RG}, \;\; Z_{MRG} = j\omega_{RG} M_G \end{aligned} \tag{12}$$

and

$$\omega_{RG} = \omega_S - N_{PG} \omega_G \tag{13}$$

Note that the number of pole pairs of the generator, denoted N_{PG}, is allowed to be different from the motor, so that the motor and generator speeds could be quite different.

3) Integrated model of the motor/generator set: The complex model of the motor/generator set is composed of the four differential equations (7) and (11), but there are only three independent (complex) states (i_S, i_R, and i_{RG}). On the other hand, the voltage v_S is an output of the system. By subtracting the stator equations, an integrated model of the motor/generator set can be obtained

$$\begin{aligned} (L_S + L_{SG}) \frac{di_S}{dt} + M \frac{di_R}{dt} - M_G \frac{di_{RG}}{dt} &= \\ -(Z_S + Z_{SG}) i_S - Z_{MS} i_R + Z_{MSG} i_{RG} & \\ M \frac{di_S}{dt} + L_R \frac{di_R}{dt} &= v_R - Z_R i_R - Z_{MR} i_S \\ -M_G \frac{di_S}{dt} + L_{RG} \frac{di_{RG}}{dt} &= v_{RG} - Z_{RG} i_{RG} + Z_{MRG} i_S \end{aligned} \tag{14}$$

A remarkable result is that, although the combination of the two machines involves twelve windings, the complex representation yields a model with only three complex variables.

III. Control of the Motor/Generator Set

A. Overall organization of the control law

The structure of the control law is shown in Fig. 2. Three reference values are provided: v_{REF} the reference value for the magnitude of the complex stator voltage v_S (in V), ω_{REF} the reference value for the speed of

the motor (in rad/s), and f_{REF}, the reference value for the frequency of the stator voltages (in Hz). The figure shows four components that are described below.

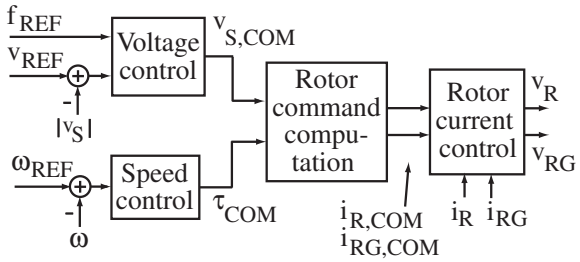

Fig. 2. Overall organization of the control law

B. Rotor current control

An inner control system is used to ensure that the rotor currents track commands $i_{R,COM}$ and $i_{RG,COM}$. Two options are considered: a voltage command mode that does not use current measurements, and a current command mode that uses current measurements to ensure tighter tracking and limiting of the rotor currents.

1) Voltage command mode: In the voltage command mode, the inner control loop is an open-loop command based on the steady-state response of the machine (which corresponds to zero derivatives). Based on (14), the rotor voltages are set to

$$\begin{aligned} v_R &= Z_R i_{R,COM} + Z_{MR} i_S \\ v_{RG} &= Z_{RG} i_{RG,COM} - Z_{MRG} i_S \end{aligned} \tag{15}$$

The drawbacks of the voltage command mode are that the system is assumed to be open-loop stable (which is not straightforward to prove for arbitrary motor and generator speeds), and that the rotor currents are not actively regulated. On the other hand, the control system is simpler, and can be useful as an intermediate step in the testing of the current command mode.

2) Current command mode: Current control laws for cage rotor induction machines are developed using the complex representation in [18], [19], [20]. The algorithm given here is similar in principle to the one presented in [20], although considerably different since the currents of two interconnected machines are controlled instead of those of a single machine. The current control loop is designed by obtaining a model involving only di_R/dt and di_{RG}/dt. Extracting di_S/dt from the first equation of (14) and substituting it in the second and third equations, the following equations are obtained

$$L_{MAT} \begin{pmatrix} \frac{di_R}{dt} \\ \frac{di_{RG}}{dt} \end{pmatrix} = \begin{pmatrix} v_R - u_R \\ v_{RG} - u_{RG} \end{pmatrix} \tag{16}$$

where

$$L_{MAT} = \begin{pmatrix} L_R - \frac{M^2}{L_S + L_{SG}} & \frac{M M_G}{L_S + L_{SG}} \\ \frac{M M_G}{L_S + L_{SG}} & L_{RG} - \frac{M_G^2}{L_S + L_{SG}} \end{pmatrix} \tag{17}$$

and

$$\begin{aligned} u_R &= Z_R i_R + Z_{MR} i_S + \frac{M\ x_R}{L_S + L_{SG}} \\ u_{RG} &= Z_{RG} i_{RG} - Z_{MRG} i_S - \frac{M_G\ x_R}{L_S + L_{SG}} \end{aligned} \tag{18}$$

while

$$x_R = (Z_S + Z_{SG}) i_S + Z_{MS} i_R - Z_{MSG} i_{RG} \tag{19}$$

The current control algorithm is then given by

$$\begin{pmatrix} v_R \\ v_{RG} \end{pmatrix} = \begin{pmatrix} u_R \\ u_{RG} \end{pmatrix} + \left(K_{PC} + \frac{K_{IC}}{s} \right) L_{MAT} \begin{pmatrix} i_{R,COM} - i_R \\ i_{RG,COM} - i_{RG} \end{pmatrix} \tag{20}$$

where K_{PC} and K_{IC} are proportional and integral gains of the control loop. Note that the PI controller is actually a two-dimensional controller applied to a vector of complex variables so that, in the real variables, there are actually four identical PI controllers regulating the two sets of three-phase rotor currents.

In ideal conditions (that is, if the model is exact), the closed-loop dynamics of the rotor currents can be obtained by converting (16) to the Laplace domain and applying the control law (20). Cancelling L_{MAT} that appears on both sides of the equation, the dynamics of the rotor currents simplify to the two (four in the real domain) decoupled second-order systems

$$\begin{pmatrix} i_R \\ i_{RG} \end{pmatrix} = \frac{K_{PC} s + K_{IC}}{s^2 + K_{PC} s + K_{IC}} \begin{pmatrix} i_{R,COM} \\ i_{RG,COM} \end{pmatrix} \tag{21}$$

For example, the poles of the current loop can be set at some desired locations $s = -a_{DC}$ by letting $K_{PC} = 2a_{DC}$, and $K_{IC} = a_{DC}^2$. The parameter a_{DC} can be interpreted as the inverse of a time constant $a_{DC} = 1/\tau$, or as a measure of the bandwidth of the current loop in rad/s. Generally, one will want to set the parameter a_{DC} as high as possible, with limits imposed by the noise on the current measurements and unmodelled dynamics in the current loop.

C. Rotor command computation

The rotor current commands are used to follow stator voltage and current commands. Defining

$$L_T = L_S + L_{SG}, \quad Z_T = Z_S + Z_{SG} \tag{22}$$

(14) gives the relationship

$$(sL_T + Z_T)\, i_S = -D_{MS}(s) i_R + D_{MSG}(s) i_{RG} \tag{23}$$

where

$$D_{MS}(s) = sM + Z_{MS},\ D_{MSG}(s) = sM_G + Z_{MSG} \tag{24}$$

On the other hand, (7) gives the stator voltage

$$v_S = (sL_S + Z_S)\, i_S + (sM + Z_{MS})\, i_R \tag{25}$$

Combining (25) with (23) and simplifying the result, one finds

$$\begin{aligned}(sL_T + Z_T)\, v_S = {} & D_{SG}(s)D_{MS}(s)i_R \\ & + D_S(s)D_{MSG}(s)i_{RG}\end{aligned} \tag{26}$$

where

$$D_S(s) = sL_S + Z_S,\ D_{SG}(s) = sL_{SG} + Z_{SG} \tag{27}$$

Then, (21), (23), and (26) yield the system response

$$\begin{pmatrix} v_S \\ i_S \end{pmatrix} = G(s) \begin{pmatrix} i_{R,COM} \\ i_{RG,COM} \end{pmatrix} \tag{28}$$

where

$$\begin{aligned}G(s) = {} & \frac{K_{PC}s + K_{IC}}{(sL_T + Z_T)\,(s^2 + K_{PC}s + K_{IC})} \\ & \begin{pmatrix} D_{SG}(s)D_{MS}(s) & D_S(s)D_{MSG}(s) \\ -D_{MS}(s) & D_{MSG}(s) \end{pmatrix}\end{aligned} \tag{29}$$

Note that the transfer function matrix $G(s)$ is stable, having the poles of the rotor current control loop and a pole at $s = -Z_T/L_T$ with negative real part. A simple approach for the rotor current command consists in setting

$$\begin{pmatrix} i_{R,COM} \\ i_{RG,COM} \end{pmatrix} = G(0)^{-1} \begin{pmatrix} v_{S,COM} \\ i_{S,COM} \end{pmatrix} \tag{30}$$

where $v_{S,COM}$ and $i_{S,COM}$ are stator voltage and current commands to be defined. The response from the stator commands to the stator variables is then determined by a stable system with a gain equal to the identity matrix at low frequencies. More advanced control laws are possible using the dynamic model (28)-(29), but were not found necessary in the experiments of the paper.

The stator current command $i_{S,COM}$ is computed from the torque command τ_{COM} shown in Fig. 2 and a set-point for the reactive power q_S transferred from the generator to the motor. Although other choices can be made, the set-point for the variable q_S is chosen to be zero to minimize the magnitude of the currents exchanged between the stators. From the model of the motor (7), (8) and (10), one can deduce that

$$\begin{aligned}\mathrm{Re}(v_S i_S^*) &= R_S\,|i_S|^2 + \omega_S M\,\mathrm{Im}\,(i_S i_R^*) \\ &= R_S\,|i_S|^2 + \frac{\omega_S\ \tau_M}{N_P}\end{aligned} \tag{31}$$

Setting $q_S = 0$, (6) implies that

$$v_S i_S^* = R_S\,|i_S|^2 + \frac{\omega_S\ \tau_M}{N_P} \tag{32}$$

Accordingly, the stator current command is set to

$$i_{S,COM} = i_{COM}\ e^{\,j\angle v_S} \tag{33}$$

where i_{COM} is a real variable that solves the quadratic equation

$$R_S i_{COM}^2 - |v_S|\, i_{COM} + \frac{\omega_S\ \tau_{COM}}{N_P} = 0 \tag{34}$$

and τ_{COM} is the torque command. The solution of (34) such that $\tau_{COM} = 0$ corresponds to $i_{COM} = 0$ is given by

$$i_{COM} = \frac{|v_S| - \sqrt{|v_S|^2 - 4R_S(\omega_S/N_P)\tau_{COM}}}{2R_S} \tag{35}$$

Note that the stator resistance R_S may be neglected for a large machine, and the current command simply becomes

$$i_{COM} = \frac{\omega_S\ \tau_{COM}}{N_P\,|v_S|} \tag{36}$$

D. Voltage control

Two references are specified by the user for this control loop: a magnitude voltage reference v_{REF} (in V) and a frequency reference f_{REF} (in Hz). v_{REF} specifies the desired value of $|v_S|$, so that $v_{REF} = \sqrt{3/2}\ v_{pk,REF}$, where $v_{pk,REF}$ is the reference value for the peak line-neutral stator voltage, as indicated by (5). The frequency reference is used to define the angular frequency of the reference frame with

$$\omega_S = 2\pi f_{REF} \tag{37}$$

and the angle of the reference frame θ_S is obtained by integrating (4).

The variable $v_{S,COM}$ is chosen to be real, which results in an alignment of the reference frame on the *commanded* stator voltage. An integral control algorithm is useful to ensure the regulation of the magnitude of the stator voltage in steady-state despite errors in the model. Specifically, we let

$$v_{S,COM} = v_{REF} + K_{IV} \int (v_{REF} - |v_S|)dt \tag{38}$$

Using $G(0)$ as an approximation for $G(s)$, $v_S = v_{S,COM}$, so that v_S is real and

$$\frac{v_S}{v_{REF}} = \frac{s + K_{IV}}{s + K_{IV}} = 1 \tag{39}$$

In practice, small errors and perturbations will be compensated by a closed-loop system having approximately the dynamics of a first-order linear time-invariant system. A desired value of $s = -a_{DV}$ is obtained by letting $K_{IV} = a_{DV}$. The full dynamics involve the transfer function matrix $G(s)$ in (29) instead of $G(0)$. To justify neglecting the dynamics of (29), the pole at $s = -a_{DV}$ should be sufficiently small (for example,

$a_{DV} \leqslant a_{DC}/10$). Note that the control law (38) was chosen to be a pure integral control law to reduce the effect of noise from the voltage measurement.

E. Speed control

A second outer control loop regulates the speed, given a speed reference ω_{REF}. The torque command is set to

$$\tau_{COM} = K_P(\omega_{REF} - \omega) + K_I \int (\omega_{REF} - \omega) dt \quad (40)$$

where K_P, K_I are proportional and integral gains of the velocity controller. For the selection of the PI gains, a model of the mechanical system of the motor should be assumed. For example, assume that the dynamics of the motor are characterized by the mechanical equation

$$J\frac{d\omega}{dt} = \tau_M - \tau_L \quad (41)$$

where J is the inertia of the motor (including the load), and τ_L is the non-inertial component of the load torque (assumed to be constant for analysis). Assuming that the torque command is tracked by the inner loop, so that $\tau_M = \tau_{COM}$, and treating the load torque as a disturbance, the closed-loop poles of the speed control loop are given by the roots of

$$Js^2 + K_P s + K_I = 0 \quad (42)$$

Both poles of the velocity loop can be set at some desired value $s = -a_D$ by letting $K_P = 2a_D J$ and $K_I = a_D^2 J$. Again, to justify neglecting the dynamics of (29), the pole at $s = -a_D$ should be sufficiently small (for example, $a_D \leqslant a_{DC}/10$). In the implementation, the term $K_P(\omega_{REF} - \omega)$ may also be replaced by $K_F K_P \omega_{REF} - K_P \omega$, where $K_F \leqslant 1$ is a parameter adjusted to move the zero of the closed-loop transfer function further into the left half-plane and avoid a possible overshoot in the responses.

F. Alternative implementation

An alternative implementation consists in replacing some of the current variables by the associated commands, which reduces the amount of noise re-injected in the system through the control law. Specifically, i_R and i_{RG} are replaced by $i_{R,COM}$ and $i_{RG,COM}$ in all the equations except (20), and i_S is replaced by $i_{S,COM}$. The overall algorithm is then composed of only a few equations in the complex domain. With the procedure as described, all the parameters of the proposed control algorithm can be specified based on *a priori* knowledge of the electrical parameters and of the motor inertia (including the load), together with desired locations for the closed-loop poles (a_{DC} for the rotor current control loop, a_{DV} for the voltage control loop, and a_D for the velocity control loop).

G. Command limiting

Command limiting is useful to ensure that:

- the algorithm is well-defined (in particular, the arguments of the square roots are positive).
- limits on the rotor currents are satisfied (to protect the machines and the rotor side converters).
- windup of the control laws is prevented.

The rotor currents are assumed to be constrained so that $|i_R| \leqslant i_{R,MAX}$ and $|i_{RG}| \leqslant i_{RG,MAX}$. Then, the following limits can be derived (the alternative implementation is assumed).

1) Voltage command limit: The rotor current limits impose a limit on the achievable stator voltage. For zero torque command, which is equivalent to $i_{S,COM} = 0$, the stator voltage is given by

$$v_S = j\omega_S M i_R \quad (43)$$

Therefore, the stator voltage command should be limited to

$$v_{S,COM} \leqslant \min(\omega_S M i_{R,MAX},\ \omega_S M_G i_{RG,MAX}) \quad (44)$$

Note that a smaller limit may be applied to leave room for a nonzero torque command. In any case, the limit should also be used to prevent windup of the voltage control loop.

2) Torque command limit: A first torque limit originates from the existence of the square root in (35), which requires

$$\tau_{COM} \leqslant \tau_{MAX,0} \triangleq \frac{N_P v_{S,COM}^2}{4R_S\omega_S} \quad (45)$$

The torque command should also be limited so that rotor current limits are observed. The result is obtained by first finding a condition on the stator current command $i_{S,COM}$, and then deriving a torque command limit.

From (25) in steady-state ($s = 0$) and where v_S, i_S, i_R are replaced by the commands

$$\begin{aligned}(v_{S,COM} - R_S i_{COM})^2 + (\omega_S L_S i_{COM})^2 \\ = (\omega_S M i_{R,COM})^2\end{aligned} \quad (46)$$

so that $|i_{R,COM}| \leqslant i_{R,MAX}$ if and only if

$$a_1 i_{COM}^2 - 2a_2 i_{COM} - a_3 \leqslant 0 \quad (47)$$

where

$$\begin{aligned}a_1 = R_S^2 + (\omega_S L_S)^2,\ a_2 = R_S v_{S,COM}, \\ a_3 = (\omega_S M i_{R,MAX})^2 - v_{S,COM}^2\end{aligned} \quad (48)$$

From (44), it follows $a_3 \geqslant 0$. An equality is obtained in (48) for

$$\begin{aligned}i_{MAX} = \frac{a_2 + \sqrt{a_2^2 + a_1 a_3}}{a_1}, \\ i_{MIN} = \frac{a_2 - \sqrt{a_2^2 + a_1 a_3}}{a_1}\end{aligned} \quad (49)$$

and (47) is satisfied when i_{COM} lies between the two limits. With (34), the result implies torque limits

$$\tau_{MAX,1} = \frac{N_P}{\omega_S}\left(v_{S,COM}\ i_{MAX} - R_S i_{MAX}^2\right)$$
$$\tau_{MIN,1} = \frac{N_P}{\omega_S}\left(v_{S,COM}\ i_{MIN} - R_S i_{MIN}^2\right) \quad (50)$$

For the generator, similar equations hold with G subscripts, but note the change of sign in $a_{G,2}$

$$a_{G,1} = R_{SG}^2 + (\omega_S L_{SG})^2,\ a_{G,2} = R_{SG} v_{S,COM},$$
$$a_{G,3} = (\omega_S M_G i_{RG,MAX})^2 - v_{COM}^2 \quad (51)$$

and

$$i_{G,MAX} = \frac{a_{G,2} + \sqrt{a_{G,2}^2 + a_{G,1}a_{G,3}}}{a_{G,1}},$$
$$i_{G,MIN} = \frac{a_{G,2} - \sqrt{a_{G,2}^2 + a_{G,1}a_{G,3}}}{a_{G,1}} \quad (52)$$

so that

$$\tau_{MAX,2} = \frac{N_{PG}}{\omega_S}\left(v_{S,COM}\ i_{G,MAX} - R_{SG} i_{G,MAX}^2\right)$$
$$\tau_{MIN,2} = \frac{N_{PG}}{\omega_S}\left(v_{S,COM}\ i_{G,MIN} - R_{SG} i_{G,MIN}^2\right) \quad (53)$$

Overall, the following torque limits are obtained

$$\tau_{MAX} = \min(\tau_{MAX,0},\ \tau_{MAX,1},\ \tau_{MAX,2})$$
$$\tau_{MIN} = \max(\tau_{MIN,1},\ \tau_{MIN,2}) \quad (54)$$

If the motor and the generator are identical machines, $\tau_{MAX,1} = \tau_{MAX,2}$ and $\tau_{MIN,1} = \tau_{MIN,2}$. Otherwise, the machines should be designed so that performance would not be significantly reduced by one of the two machines.

H. Modifications and enhancements

The following adjustments may also be made:
(a) For a large machine, a reasonable approximation consists in setting $R_S = 0$. This approximation was applied in (36), and could also be used to simplify other equations.
(b) In the derivations, the inductances were assumed to be constant. Alternatively, the inductances could be computed as functions of the magnetizing current, using data on the saturation curve of the machines.
(c) A closed-loop control system could be designed for the intermediate rotor command computation using the transfer function matrix $G(s)$.

I. Benefits of the complex representation

The dimension of the complex representation is smaller than the real representation by a factor of 2. The model is not an approximation, but rather a compact representation of the system. The algorithm of the paper could have been derived in the real domain. The equations would be similar, except that two-dimensional vectors would replace the complex variables. Some of the parameters could remain scalar, but would generally need to become multiples of the identity matrix (such as the inductances L_S, M, ...). Other parameters would become non-diagonal matrices (such as the impedances Z_S, Z_{MS}, $\cdots$). The matrix L_{MAT} would become a block-diagonal matrix of dimension 4.

Some steps of the derivations are simplified in the complex domain. For example, division by a complex number replaces the multiplication by the inverse of a 2x2 matrix. In transfer functions, the denominator polynomial replaces the determinant of a polynomial matrix. The product of two complex variables commutes, but this result with real matrices is not automatically known to be true. With some familiarity, derivations become streamlined and facilitated in the complex domain.

IV. Experiments

A. Experimental testbed

The algorithm was tested on an experimental testbed at the University of Utah. The main components and connections of the system are shown on Fig. 3. A dSPACE DS1104 constituted the data acquisition and control system system. The dSPACE system was programmed in Matlab/Simulink. A Hirel Systems inverter board included the two rotor side converters, whose output voltages were applied to the rotors (v_R and v_{RG}). The generator (DFIG) was connected mechanically to a brush DC motor, which served as a prime mover. A constant voltage was applied to the motor, and the voltage was varied along a pre-specified profile to increase or reduce the speed of the generator without precise regulation.

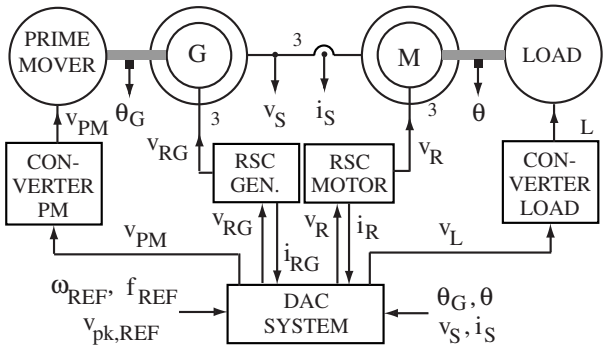

Fig. 3. Main components and connections of the experimental testbed

Machine parameters		
Stator resistance	R_S	0.66 Ω
Rotor resistance	R_R	1.07 Ω
Stator inductance	L_S	12.7 mH
Rotor inductance	L_R	8.5 mH
Mutual inductance	M	8.7 mH
Number of pole pairs	N_P	2
Motor inertia	J	3.5 10^{-4} kg m^2

TABLE I
LIST AND VALUES OF MACHINE PARAMETERS

Controller parameters		
Desired pole for velocity loop	a_D	100 rad/s
Desired pole for voltage loop	a_{DV}	100 rad/s
Desired pole for current loop	a_{DC}	1000 rad/s
Feedforward gain	K_F	2/3
Maximum rotor current	$i_{R,MAX}$	$\sqrt{3/2}$ 6 A
Inverter switching frequency	f_{SW}	10 kHz
Sampling frequency	f_S	2 kHz

TABLE II
LIST AND VALUES OF CONTROLLER PARAMETERS

The motor (DFIM) was connected mechanically to a squirrel-cage induction generator (SCIG), which served as a load. In some experiments, a DC voltage v_L was applied to the windings of the SCIG to increase the load torque. The stators of the DFIG and DFIM were connected through two current sensors and to a voltage reduction network for voltage measurement (i_S and v_S). The DC motor connected to the DFIG was driven by a third inverter on the Hirel board and provided the generator position measurement θ_G. The SCIG connected to the DFIM had an encoder that was used to read the DFIM position θ. The reference values for the speed (ω_{REF}), the stator frequency (f_{REF}), and the peak line-neutral stator voltage ($v_{pk,REF}$) were applied by the operator through a graphical interface, or pre-programmed for data collection.

The two doubly-fed induction machines were of the same model, rated at 30 V, 250 W. The electrical parameters of the doubly-fed induction motor were estimated through standstill measurements, with the values listed in Table I. The same parameters were used in the control algorithm for the generator and for the motor. The inertia of the doubly-fed induction motor and the inertia of the load (the SCIG) were estimated separately by a least-squares algorithm using acceleration data, and the inertias were summed to yield the inertia listed in the table. The controller parameters are listed in Table II. Torque limits (54) were computed in the code to limit the rotor currents and integrated with anti-windup protection.

B. Experimental results

1) Large reference steps: The first set of results was obtained with the voltage command mode. Fig. 4 shows the velocity of the motor (solid line) as well as the speed reference (dashed line) that was applied to the velocity controller. The velocity ramped up to about 1,800 rpm, maintained that value for 1.75 seconds, and then climbed to 3,600 rpm. After a second, the speed reference decreased along a similar profile. The rate of variation of the speed was deliberately limited, but was sufficiently high to exceed the torque capability of the motor in the first part of the profile. In the rise from 1,800 rpm to 3,600 rpm, it was found that the rate had to be limited to avoid tripping the DC power supply providing power to the experiment. As a result, the motor followed closely the reference for the remainder of the profile.

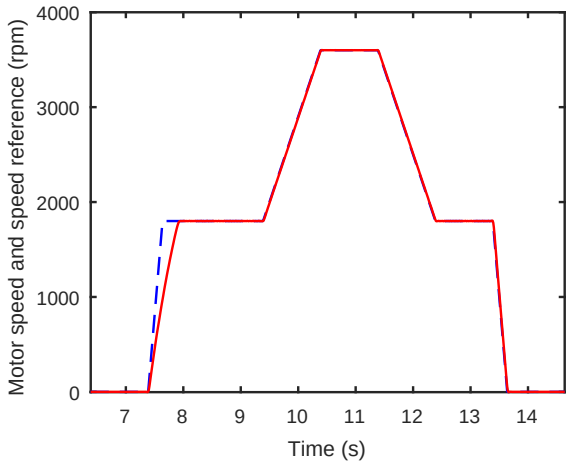

Fig. 4. Motor speed (solid) and speed reference (dashed)

Fig. 5 shows the peak stator voltage. The voltage is an instantaneous, line-neutral, peak value obtained using the estimate $v_{pk} = \sqrt{2/3}\,|v_S|$. The reference voltage is not shown because it is the piecewise linear function that can easily be deduced from the figure. Tracking of the reference voltage is excellent, even when the speed of the motor suddenly rises or falls.

Fig. 6 shows the velocity of the generator, which starts at 1,800 rpm, then is increased when the speed reference of the motor is raised. The dashed line shows the reference frequency of the generated voltage divided by N_P and multiplied by $30/\pi$, which is the synchronous speed (in rpm) for the motor and the generator since $N_P = N_{PG}$. Note that the speed is not regulated exactly, but is determined by the voltage applied to the DC motor driving the generator, together with the load drawn by

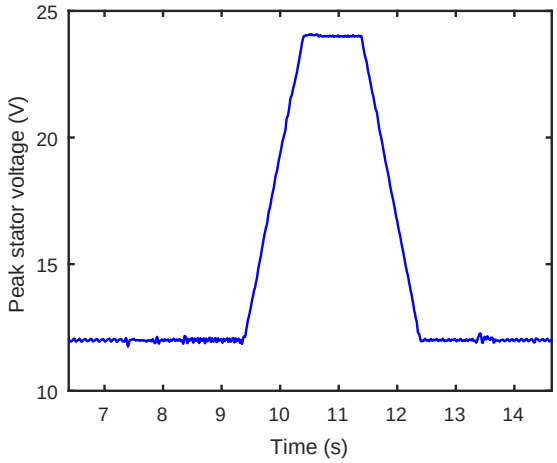

Fig. 5. Peak stator voltage

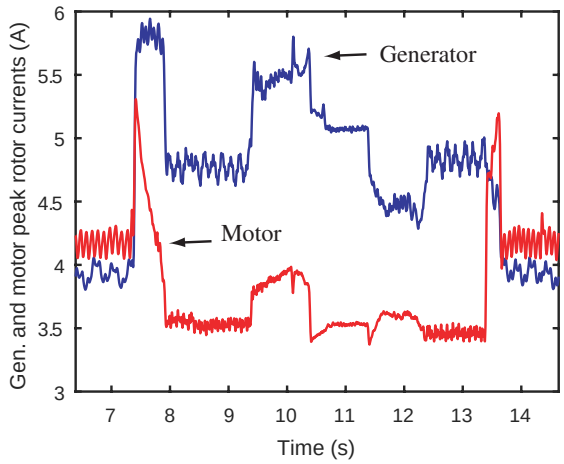

Fig. 7. Peak rotor currents for the generator and the motor

the motor. The generator operates in a sub-synchronous mode for most of the experiment, with a brief super-synchronous period when the motor rapidly decelerates at the end. On the other hand, the motor starts in the sub-synchronous mode at 100% slip and shifts between sub- and super-synchronous modes during the experiment.

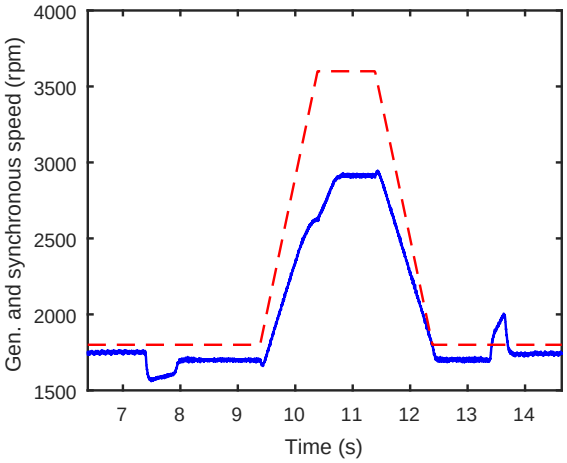

Fig. 6. Generator speed (solid) and stator reference frequency expressed as an equivalent synchronous speed (dashed)

Fig. 7 shows the peak rotor currents, obtained using a similar formula as for the stator voltages. The current is larger for the generator, and reaches a peak close to the imposed limit of 6 A through (54).

Fig. 8 shows the torque command, as well as the upper and lower torque limits computed in real-time using the formulas. As expected from the velocity and rotor current plots, the upper torque limit is reached during the rapid acceleration phase between 7 and 8 seconds.

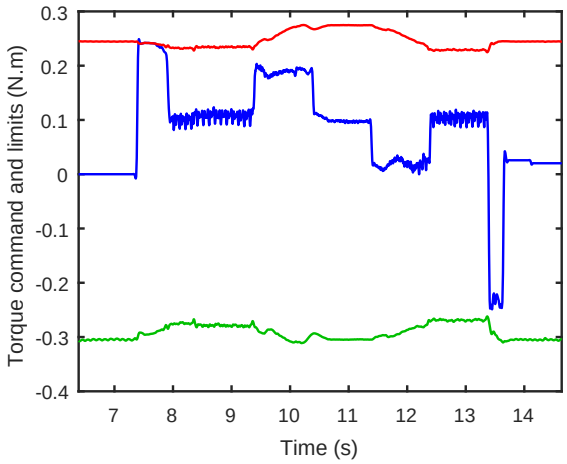

Fig. 8. Torque command with upper and lower torque limits computed by the algorithm

Fig. 9 shows the active and reactive powers absorbed by the motor through the stator. The reactive power is not actively regulated to zero, but is nevertheless small. As expected, the active power becomes greater at higher speeds and during periods of rapid acceleration. There is a brief period of regeneration during the fast braking period between 13 and 14 seconds, which causes the generator to become super-synchronous in Fig. 6.

Fig. 10 compares the velocity response for the voltage command and current command modes. The overall response with the current command is very similar to the voltage command mode in Fig. 5. Fig. 10 shows a close-up during the first acceleration period where a small difference is visible. One finds that the current command mode provides a slighly faster acceleration rate than the voltage command mode.

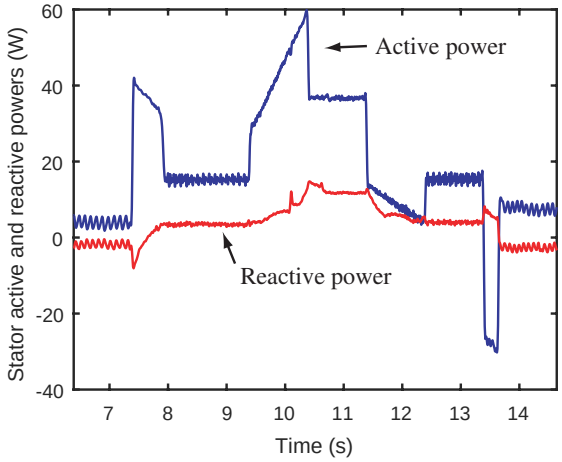

Fig. 9. Stator active and reactive powers absorbed by the motor

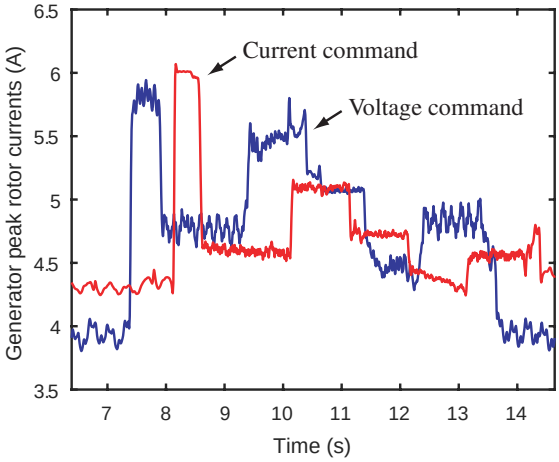

Fig. 11. Peak rotor currents in voltage command mode and current command mode

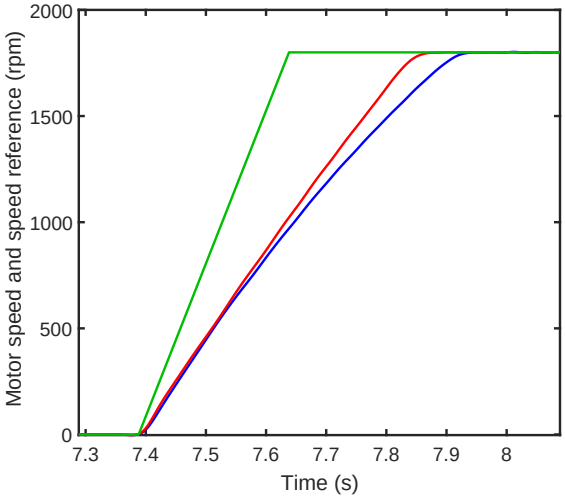

Fig. 10. Velocity response in voltage command and current command

Fig. 11 shows the peak rotor currents in the voltage command and the current command modes. The current command response is shifted by a second to avoid overlap of the responses. One finds that the current command mode better exploits the full capability of the motor, which explains the slightly faster response of Fig. 10. In other situations, it is possible that the voltage command mode would result in slightly faster response, but at the price of exceeding the rotor current limit. The main advantage of the current command mode is not the small increase of performance seen in Fig. 10, but the ability to limit the peak current to specified limits despite uncertainties in the machine models.

2) Dynamic responses: Fig. 12 shows the response to a torque command τ_{COM}. The machine was started using the current command and, in steady-state, the torque command was replaced by a value that sustained the speed at its setting of 1,800 rpm. Afterwards, positive and negative steps with magnitude 0.1 N m and 0.15 N m were applied. The speed rises and decreases linearly as expected from (41). During the first pulse, the speed rises to 1,870 rpm in 0.03 seconds. The 244 rad/s^2 acceleration with a torque command of 0.1 N m suggests an inertia of 4.1 10^{-4} kg m^2, slightly larger than the inertia listed in Table I. It is possible that the actual inertia is larger than the estimate, or that the applied torque is slightly smaller than the torque command. Also note that, because the friction is mostly due to Coulomb friction in the system and does not vary much with speed, the motor speed does not return exactly to its original value at the end of the run, even though the torque command does.

Fig. 13 shows the responses to positive and negative steps in speed reference, peak stator voltage reference, and frequency reference using the current command mode. The red curve shows the response and the dashed blue curve shows the reference value. The frequency is an estimate of the instantaneous frequency obtained off-line. In all cases, first-order responses with time constants of the order of 10 ms are observed, consistent with the setting of the closed-loop poles at $a_D = a_{DV} =$ 100 rad/s. Only small couplings are observed between the variables.

Fig. 14 shows the torque command and speed responses to increments of load. The load torque was increased by applying a DC voltage from phase A of the three-phase SCIG to phases B and C connected together. On the torque command plot, the blue curve is the DC voltage scaled to match the plot. The increase in torque command is about 0.1 N m from a baseline torque of 0.082 N m due to friction. The load torque based on

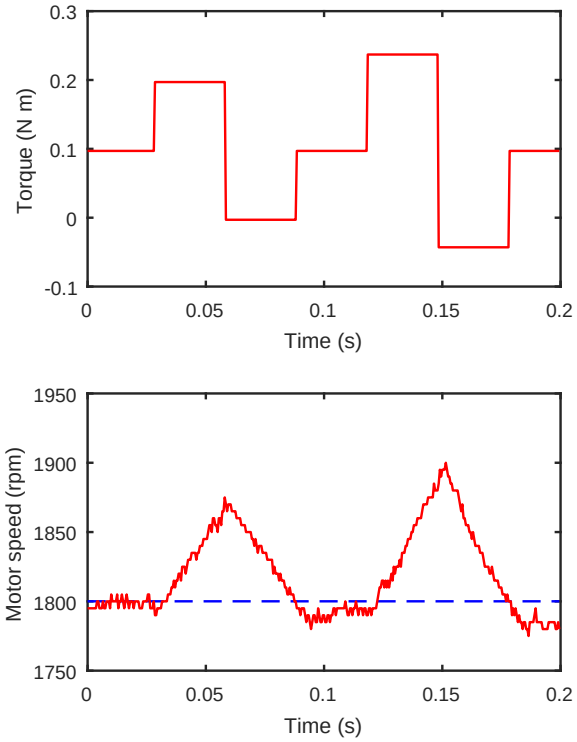

Fig. 12. Speed response to an open-loop torque command

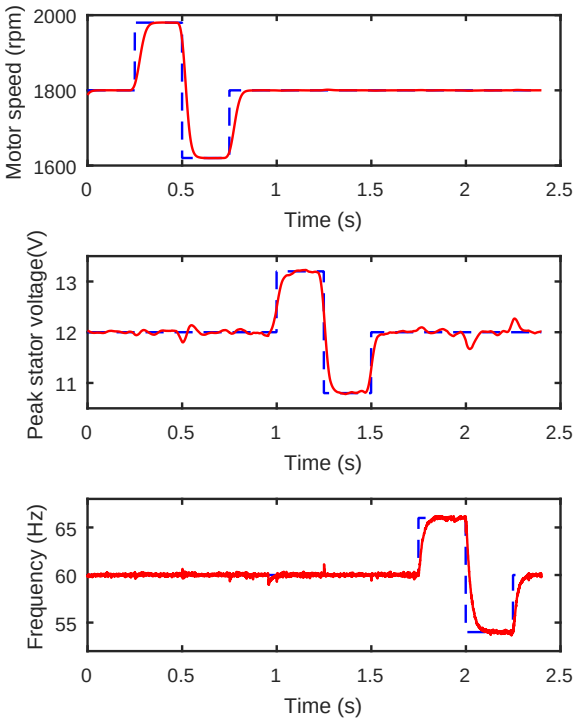

Fig. 13. Responses to steps of speed reference, peak stator voltage reference, and frequency reference

estimates of the parameters of the induction machine was computed to be 0.088 N m. The bottom of Fig. 14 shows that the speed is rapidly brought back to the nominal value with small transient deviations, and consistent with the time constant of 10 ms observed in other responses.

V. Implementation Issues

The proposed integrated motor/generator control system constitutes the inner component of a larger control system that remains a subject of future research. For a fully functional system, an outer loop would need to set the reference values for the speed of the prime mover, the speed for the motor, the stator voltage magnitude, and the stator voltage frequency. The objective of the higher level of control would be to optimize the tracking performance and the efficiency of the system while, as importantly, satisfying the constraints on the components of the system. Among these constraints, one should consider:

(a) the amount of stored energy. Neglecting losses, (7) and (11) imply that the powers absorbed by the rotors in steady-state are given by

$$P_R = -\left(\omega_R/\omega_S\right) P_S, \quad P_{RG} = \left(\omega_{RG}/\omega_S\right) P_S \tag{55}$$

where P_S is the power absorbed by the stator of the motor. In wind turbines, operation with a normalized slip ω_R/ω_S equal to -0.3 implies that power is generated by the rotor and is equal to 30% of the power generated by the stator. The rotor power is converted by the rotor side converter and transmitted to the grid with the stator power. In an aircraft, operation would occur most of the time at constant speed and cruising altitude. Super-synchronous operation at 30% slip for the motor and the generator would probably be a desirable mode of operation as well. In this case, power would simply be exchanged between the rotors. In other conditions, power would need to be transferred in and out of the storage element. Increasing the speed of the generator while leaving other variables constant could be a means of recharging the battery. The energy storage element could also be connected to the AC bus through a separate converter, as proposed in [4], and the control strategy would need to be adjusted accordingly.

(b) the rotor voltage constraints. Slip needs to be limited to satisfy the constraints on the rotor side converters. Neglecting the stator and rotor resistances, (7) in steady-state gives

$$v_S = j\omega_S \left(L_S i_S + M i_R\right), \quad v_R = j\omega_R \left(L_R i_R + M i_S\right) \tag{56}$$

Neglecting the leakage in the machine, so that $L_S L_R \simeq$

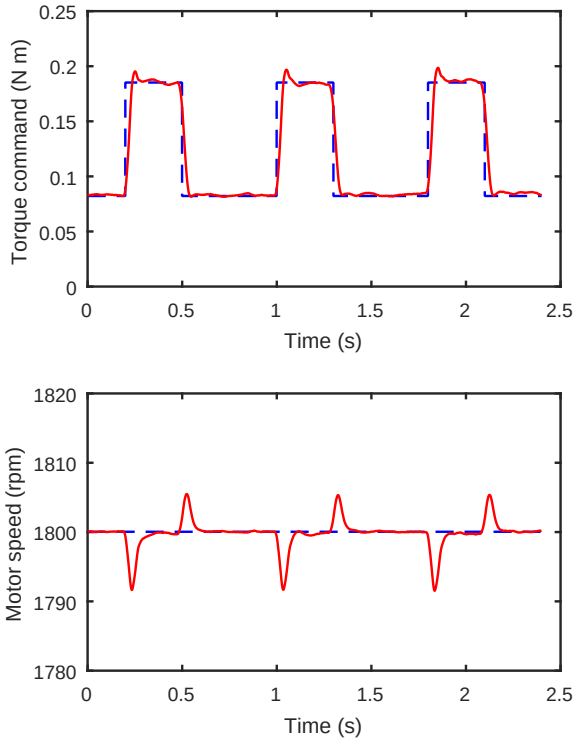

Fig. 14. Responses to steps of load torque

M^2,

$$v_R = j\omega_R \frac{M}{L_S}\left(\frac{L_S L_R}{M} i_R + L_S i_S\right) \simeq \frac{\omega_R}{\omega_S}\frac{M}{L_S} v_S \quad (57)$$

In grid-tied induction generators, the normalized slip ω_R/ω_S is limited (typically to 0.3 in magnitude), so that the rotor voltage is a fraction (30%) of the stator voltage reflected to the rotor (Mv_S/L_S). Controlling the slip is important in the application of this paper, but the stator voltage is a free variable that may help to satisfy the constraints. In the experiments, the motor was started at 100% slip, but with half the stator voltage.

An optimized scheme to set the reference values and satisfy the limits is left as a subject of future research. A fully coordinated control algorithm would also integrate the control of the motor/generator set with the control of the prime mover. Dynamics of the prime mover would be taken into account. There are several degrees of freedom in the system, but many constraints as well. The constraints would need to be considered during operation, as well as in the design of the system.

The challenges in making the system of Fig. 1 work make the full DC/DC conversion approach attractive. This option has fewer constraints and enables the use of machines with higher power-to-weight ratio. However, the solution is not without challenges either. DC storage would still be necessary for transient power needs, and two full power converters would be required, as opposed to two partially rated converters. Not only would there be greater losses in the power transfer, but also greater needs for cooling of the power electronics. The extra cooling would require extra weight and present particular challenges in the aircraft application.

An advantageous feature of the DFIG/DFIM option is also in terms of fault-tolerance. If the RSC converter of the doubly-fed induction motor failed in the architecture of Fig. 1, the motor could still be operated as a conventional induction machine by short-circuiting the rotor windings. A similar option would not be feasible for the full DC/DC architecture with a synchronous motor.

A major technological challenge for the DFIG/DFIM system in aircraft is the need for slip rings. This feature would limit operation to low altitudes (possibly for UAV missions), unless new solutions were developed. Otherwise, a possibility is the use of brushless doubly-fed machines, which have been the subject of much research recently. In particular, the dynamic models of brushless doubly-fed reluctance machines are the same as those used in this paper and the machines could be controlled using the same methods [21] [22].

VI. Conclusions

The paper proposed a method for the integrated control of a motor/generator set composed of two doubly-fed induction machines. A core contribution of the paper was the derivation of a model that accounted for the stator voltages and currents of the motor and of the generator being identical in the parallel AC connection (with a sign reversal for the currents). A representation with complex variables simplified the derivations considerably, resulting in a state-space description with only three state variables. Two control algorithms were derived from the model, the first called voltage command mode, and the second current command mode, with the latter requiring rotor current measurements.

Experimental results showed that the methods were effective at controlling the speed of the motor along a speed reference. The voltage and frequency of the stator variables were closely regulated, and the reactive power transferred from the generator to the motor was approximately zero. The algorithm required few computations, and the voltage command mode required only measurements of motor and generator positions. In the current command mode, improved responses and tighter current limiting could be achieved. Even so, the voltage command mode could be useful for initial testing of the hardware platform, or for continued operation after current sensor failures.

The motor/generator set of Fig. 1 can be interpreted as a variable speed transmission, converting mechanical power at one speed to power at a lower or higher speed. Control of the motor's speed is achieved electronically through the rotors of the machines. This powerful result is obtained thanks to the remarkable capabilities of doubly-fed induction machines. We hope that the developments of this paper may encourage the incorporation of doubly-fed induction machines in hybrid electric aircraft, and perhaps other applications as well.

VII. Acknowledgment

The authors thank the NASA Glenn Research Center and the Universities Space Research Association for their support of this project. The leadership provided by Ray Beach and Linda Taylor is much appreciated, as well as the technical interactions with David Sadey, Keith Hunker, Jeff Csank, and Dr. Susan Frost. The authors also thank Linda Taylor for providing comments on the paper, and Bhavana Mukunda and Logan Affleck for performing preliminary experiments. Logan Affleck's contribution in building some hardware components of the testbed was also very valuable. The authors also thank the reviewers for many constructive comments that contributed to improving the paper.

References

[1] D. J. Sadey, L. M. Taylor, & R.F. Beach, "Proposal and development of a high voltage variable frequency alternating current power system for hybrid electric aircraft", *14th International Energy Conversion Engineering Conference*, Salt Lake City, UT, July 2016.

[2] S. Muller, M. Deicke, & R. W. De Doncker, "Doubly fed induction generator systems for wind turbines," *IEEE Industry Applications Magazine*, vol. 8, no. 3, pp. 26-33, 2002.

[3] J. Hou, J. Sun & H. Hofmann, "Integrated control of power generation, electric motor and hybrid energy storage for all-electric ships," *2016 American Control Conference (ACC)*, Boston, MA, 2016, pp. 6797-6802.

[4] R. Peña, R. Cárdenas, J. Proboste, J. Clare, & G. Asher, "Wind–diesel generation using doubly fed induction machines," *IEEE Transactions on Energy Conversion*, vol. 23, no. 1, pp. 202-214, 2008.

[5] D. J. Sadey, M. Bodson, J. T. Csank, K. R. Hunker, C. J. Theman, & L. M. Taylor, "Control demonstration of multiple doubly-fed induction motors for hybrid electric propulsion," *AIAA Propulsion and Energy Forum*, Atlanta, GA, July 2017.

[6] M. Bodson, D. J. Sadey, K. R. Hunker, C. J. Theman, L. M. Taylor, & J. T. Csank, "Hybrid Electric Propulsion Using Doubly-Fed Induction Machines," to appear in *AIAA Journal of Propulsion and Power* (available on-line), 2019.

[7] D.W. Novotny & J.H. Wouterse, "Induction machine transfer functions and dynamic response by means of complex time variables," *IEEE Transactions on Power Apparatus and Systems*, vol. 95, no. 4, pp. 1325-1335, 1976.

[8] L. Harnefors, "Modeling of three-phase dynamic systems using complex transfer functions and transfer matrices," *IEEE Transactions on Industrial Electronics*, vol. 54, no. 4, pp. 2239-2248, 2007.

[9] O. Troeng, B. Bernhardsson & C. Rivetta, "Complex-coefficient systems in control," *2017 American Control Conference (ACC)*, Seattle, WA, 2017, pp. 1721-1727.

[10] M. Menaa, O. TouhamiI, R. Ibtiouen, & M. Fadel, "Speed sensorless induction motor control using extended complex Kalman filter and spiral vector model," *6th WSEAS International Conference on Power Systems*, Lisbon, Portugal, 2006, pp. 261-266.

[11] M. Bodson, "Design of controllers in the complex domain," *IEEE Conference of Decision and Control*, Los Angeles, CA, 2014, pp. 4077-4082.

[12] H. J. Baesmat & M. Bodson, "Pole placement control for doubly-fed induction generators using compact representations in complex variables," *IEEE Transactions on Energy Conversion*, vol. 34, no. 2, pp. 750-760, 2019.

[13] Y. Ren, D. Su & J. Fang, "Whirling modes stability criterion for a magnetically suspended flywheel rotor with significant gyroscopic effects and bending modes," *IEEE Transactions on Power Electronics*, vol. 28, no. 12, pp. 5890-5901, 2013.

[14] A. Dòria-Cerezo & M. Bodson, "Design of controllers for electrical power systems using a complex root locus method," *IEEE Transactions on Industrial Electronics*, vol. 63, no. 6, pp. 3706-3716, 2016.

[15] M. Bodson & O. Kiselychnyk, "The complex Hurwitz test for the analysis of spontaneous self-excitation in induction generators," *IEEE Transactions on Automatic Control*, vol. 58, no. 2, pp. 449-454, 2013.

[16] A. Dòria-Cerezo, M. Bodson, C. Batlle, & R. Ortega, "Study of the stability of a direct stator current controller for a doubly fed induction machine using the complex Hurwitz test," *IEEE Transactions on Control Systems Technology*, vol. 21, no. 6, pp. 2323-2331, 2013.

[17] M. Bodson, "Speed control for doubly fed induction motors with and without current feedback," to appear in *IEEE Transactions on Control Systems Technology* (available in early access on ieeexplore, 2019).

[18] D. W. Novotny & T. A. Lipo, *Vector Control and Dynamics of AC Drives*, Oxford University Press, NY, 1996.

[19] F. B. del Blanco, M. W. Degner, & R. D. Lorenz, "Dynamic analysis of current regulators for AC motors using complex vectors," *IEEE Transactions on Industry Applications*, vol. 35, no. 6, pp. 1424-1432, 1999.

[20] S.-K. Sul, *Control of electric machine drive systems*, Wiley, Hoboken, NJ, 2011.

[21] T. D. Strous, H. Polinder, & J. A. Ferreira, "Brushless doubly-fed induction machines for wind turbines: developments and research challenges," *IET Electric Power Applications*, vol. 11, no. 6, pp. 991-1000, 2017.

[22] W. K. Song, D. G. Dorrell, A. M. Knight, R. E. Betz, & D. Gay, "Operating limits and practical operation of a brushless doubly-fed reluctance machine," *2017 IEEE Energy Conversion Congress and Exposition (ECCE)*, Cincinnati, OH, 2017, pp. 5846-5852.